Charge and Zener polaron order in $Bi_{0.75}Sr_{0.25}MnO_3$

Carlos Frontera and José Luis García-Muñoz
Institut de Ciència de Materials de Barcelona, CSIC, Campus Universitari de Bellaterra, E-08193 Bellaterra, Spain

Miguel A. G. Aranda
Dep. Cristalografía y Mineralogía, Univ. de Málaga, 29071 Málaga, Spain

Maryvonne Hervieu
Laboratoire CRISMAT, UMR associée au CNRS, ISMRA, 6 Boulevard Maréchal Juin, 14050 Caen Cedex, France

Clemens Ritter
Institut Laue Langevin, 6, rue Jules Horowitz, F-38042 Grenoble Cedex 9, France

Lluís Mañosa
Dep. d'Estructura i Constituents de la Matèria, Facultat de Física, Universitat de Barcelona, Avinguda Diagonal 647, E-08028 Barcelona, Spain

Xavier G. Capdevila and Albert Calleja
Dep. d'Enginyeria Química i Metal·lúrgia, Universitat de Barcelona, Facultat de Química, c\ Martí i Franquès 1, E-08028 Barcelona, Spain

(Received 6 February 2003; revised manuscript received 23 May 2003; published 7 October 2003)

We have characterized the RT structure of $Bi_{0.75}Sr_{0.25}MnO_3$ by means of electron diffraction, synchrotron x-ray, and neutron powder diffraction. These data evidence that $a \sim b \sim \sqrt{2}a_p$ and $c \sim 2a_p$ average structure presents a modulation that doubles the *a* and *c* lattice parameters. The temperature evolution of this compound above RT has been investigated using magnetization, calorimetry measurements, and neutron powder diffraction. These data reveal that the superstructure disappears above ~575 K where a structural transition takes place. Susceptibility data show that, concomitant to the formation of the superstructure (on cooling), there is an enhancement of the effective paramagnetic moment as has also been found in other Bi-(Sr,Ca)MnO_3 bismuth manganites. The observed features and cell evolution signals that a new type of charge and polaron ordering occurs at this composition.

DOI: 10.1103/PhysRevB.68.134408 PACS number(s): 71.27.+a, 71.38.Ht, 71.30.+h

I. INTRODUCTION

The phenomena of charge ordering (CO) and the formation of modulated structures is one of the most studied phenomena in mixed-valence manganites ($R_{1-x}A_xMnO_3$, R ≡ rare earth A≡Ca, Sr). From the early study of Goodenough, in half doped manganites, CO has been understood as the real-space ordering of Mn^{3+} and Mn^{4+} ions forming a Wigner crystal,[1] in a way similar to the Verwey transition in magnetite.[2] It has been argued that there are mainly two energy terms contributing to the stabilization of CO: the minimization of the Coulomb repulsion, and the reduction of the elastic energy coming from the accommodation of the Jahn-Teller distortions of Mn^{3+} ions due to orbital order (OO, an ordered occupancy of d_{z^2} or $d_{x^2-y^2}$ e_g orbitals) concomitant with CO. Generally, CO/OO states compete with ferromagnetic metallic (FMM) states. The latter are favored by the reduction of the kinetic energy of e_g electrons when their mean free path enlarges. As far as the bandwidth of the e_g electrons is governed by steric effects, the Mn-O-Mn bond angle governs the transfer integral between e_g(Mn)-$2p_\sigma$(O)-e_g(Mn) orbitals.[3,4] The mean size of R and A cations ($\langle R_A \rangle$) is thus governing the competition between CO/OO and FMM states. The ionic picture of CO proposed by Goodenough was initially corroborated by means of synchrotron x-ray powder diffraction,[5,6] and later on by means of neutron powder diffraction,[7,8] but, in both cases, data were refined imposing hard constraints. Usually, two features are taken as unquestionable signs of the presence of CO. The first one is the presence of superlattice spots or peaks in electron-diffraction and powder diffraction patterns. These spots or peaks signal the existence of a subtle supercell modulation superimposed to the average cell of shorter period. The second one is the stabilization, at low temperature, of a CE-type antiferromagnetic structure. When the doping level *x* is not the ideal value 1/2, a great asymmetry between underdoped (excess of Mn^{3+}) and overdoped (excess of Mn^{4+}) cases has been extensively reported in the literature. In the former case it has been interpreted that the excess of e_g electrons are randomly located in the Mn places occupying d_{z^2} orbitals perpendicular to the planes. This implies that the superstructure formed does not change with respect to the $x=1/2$ case. These d_{z^2} orbitals introduce a ferromagnetic coupling between the planes that stabilizes the *pseudo*-CE-type magnetic structure.[9] In contrast, in the overdoped region, the excess of holes changes continuously the propagation vector describing the superstructure.[10] This drives to the characteristic charge and magnetic order for the rational value $x=2/3$.[11,12]

Although the ionic picture of CO (Mn^{3+}/Mn^{4+}) proposed by Goodenough (Ref. 1) is, at present, widely accepted, a series of papers, both theoretical and experimental, evidencing the deficiencies of this picture have appeared. In fact a first indication that this ionic picture must not be completely accurate can be found in Radaelli's work where the reported Mn-O bond distances for Mn^{3+} and Mn^{4+} are more similar than expected.[5] This disagreement with the hypothesis of Goodenough CO model can also be found in other works refining the superstructure.[6–8] In some of these works the situation is even worse and the same size for hypothetical Mn^{3+} and Mn^{4+} is obtained.[7] Other evidences against the CO picture are the x-ray absorption near-edge structure where a unique edge is found (instead of two) thus indicating a unique valence of Mn.[13]

Very recently, with the aid of single-crystal neutron-diffraction data, a new picture has been depicted.[14–16] The CO model proposed by Radaelli *et al.* in Ref. 5 fails in the refinement of these data. Interestingly, the successful refinement indicates that e_g electrons are not confined in a single Mn ion (ruling out the Mn^{3+} configuration) but they are located in a Mn-O-Mn triad with a quite open Mn-O-Mn bond angle. These two neighboring Mn ions thus present a mixed valence state $3.5+$. The shared electron couples ferromagnetically both Mn ions through the double exchange Zener mechanism forming a Zener polaron (ZP). These ZP's are spatially ordered, thus forming a ZP ordered (ZPO) phase. This order naturally induces the characteristic structural modulation of the so called CO phase. The formation of the CE-type magnetic structure is also explained by this model, but it implies a high amount of frustrated bonds. For the underdoped region the scheme proposed by the same group is quite amazing. For that region, it is proposed that two ZP's placed in consecutive stacking planes (one above the other) decompose forming two Mn^{3+} ions and one ZP pointing in between the planes.[17] Each ZP formed by this mechanism (called ZP_c, because it points to c axis in the $Pbnm$ setting) introduces a FM coupling between four consecutive planes, and the formation of Mn^{3+} reduces considerably the magnetic frustration. The consequence is the stabilization of the pseudo-CE structure found in the underdoped region.[9,18] More recently, by means of resonant x-ray-diffraction measurements, an incomplete charge disproportionation $Mn^{3.5-\delta}$-$Mn^{3.5+\delta}$ with $\delta \ll 0.5$ has been proposed but, in fact, authors were not able to set a lower limit of δ.[19]

Besides this general new ZPO picture, other recent unexpected findings related to the CO, and to the effect of $6s^2$ lone pair of Bi^{3+} ions, were found in Bi-Sr manganites. Although Bi^{3+} presents an ionic radius similar to that of La^{3+}, the ground state of $Bi_{0.5}Sr_{0.5}MnO_3$ is still controversial. Its transition temperature (T_{CO} or $T_{ZPO} \simeq 525$ K, the greatest ever reported in half doped manganites) and structural characterization suggest that the $6s^2$ lone pair is only weakly screened in this compound;[20,21] a situation different, for instance, to $Bi_{0.5}Ca_{0.5}MnO_3$ ($T_{CO} \simeq 325$ K).[20,22] Theoretical studies indicate that when the lone pair is weakly screened $6s$-Bi orbitals can hybridize with $2p$-O orbitals thus reducing the mobility of Mn e_g electron through Mn-O-Mn bridges.[23]

With the objective of exploring the unknown phase diagram of $Bi_{1-x}Sr_xMnO_3$ family, we present here an investigation of the temperature-dependent electronic behavior of $Bi_{3/4}Sr_{1/4}MnO_3$. Based on electron diffraction and neutron and synchrotron powder-diffraction measurements up to 750 K, our data confirm a singular behavior of $Bi_{3/4}Sr_{1/4}MnO_3$ compared to any other $R_{3/4}A_{1/4}MnO_3$. The results obtained are discused in the framework of CO and ZPO models.

II. EXPERIMENTAL DETAILS

A polycrystalline sample of $Bi_{0.75}Sr_{0.25}MnO_3$ has been synthesized by sol-gel method. Stoichiometric quantities of Bi_2O_3 (99.9%, Quality Chemicals), MnO_2 (99.99%, Quality Chemicals), and $SrCO_3$ (99.99%, DIOPMA) were dissolved in concentrated nitric acid. The solution was then gellified according to the acrylamide polymerization method,[24] and subjected to self-ignition. The quality of the sample was initially checked by laboratory x-ray powder diffraction. The sample is very well crystallized and only very small traces (less than 2%) of Bi_2O_3 and Mn_3O_4 (hausmannite) have been detected.[25]

Thin specimens for transmission electron microscopy were prepared simply by crushing the sample with an agate mortar and pestle. Crushed fragments were mixed with alcohol, and the small flakes deposited on a holey carbon film, supported on a copper grid. The reconstruction of the reciprocal space was carried out at room temperature with a JEOL 200CX electron microscope, working at 200 kV and equipped with an energy dispersive spectroscopy (EDS) analyzer.

Neutron powder diffraction (NPD) measurements were carried out on the D2B high-resolution diffractometer (ILL, Grenoble) in the $10'$ collimation mode using $\lambda = 1.594$ Å. Data were collected at several temperatures on heating: 300,500,525,575,600, and 750 K. Synchrotron x-ray powder diffraction (SXRPD) measurements were done on the BM16 ultra-high-resolution diffractometer (ESRF, Grenoble). A short wavelength [$\lambda = 0.540092(1)$ Å] was selected with the double-crystal Si(1 1 1) monochromator and calibrated with Si NIST. In order to minimize the x-ray absorption due to the high absorption coefficient of the compound, the sample was mixed with diamond powder and placed in a thin borosilicate glass capillary ($\phi = 0.3$ mm). For both diffractometers (D2B and BM16), the instrumental resolution function was obtained from a pattern of $Na_2Ca_3Al_2F_{14}$.

Magnetic measurements have been done in a Quantum Design superconducting quantum interference device magnetometer under an applied field of 1 T in the range 300 K $\leqslant T \leqslant$ 660 K. Differential scanning calorimetry (DSC) measurements have been performed using a TA-Instruments commercial calorimeter (model 2920) using a temperature ramp of ± 5 K/min.

III. RESULTS

Figure 1(a) shows the temperature dependence of the DC magnetic susceptibility and its inverse. A clear anomaly can be appreciated to start (on cooling) at 600 K. This anomaly is

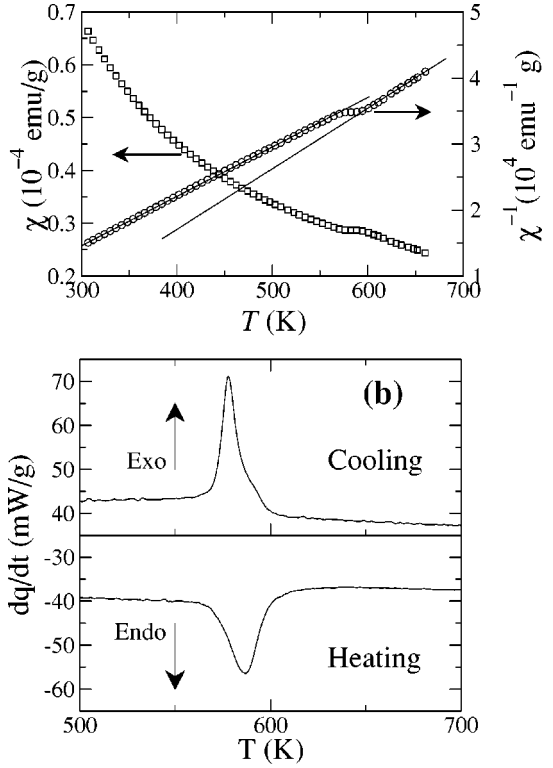

FIG. 1. (a) Temperature dependence of the susceptibility (χ) and its inverse. The straight lines are the best fit of the Curie law for the regions above and below the transition. (b) DSC thermogram showing the exotermic and endothermic transitions on cooling and heating, respectively. A small hysteresis can be observed.

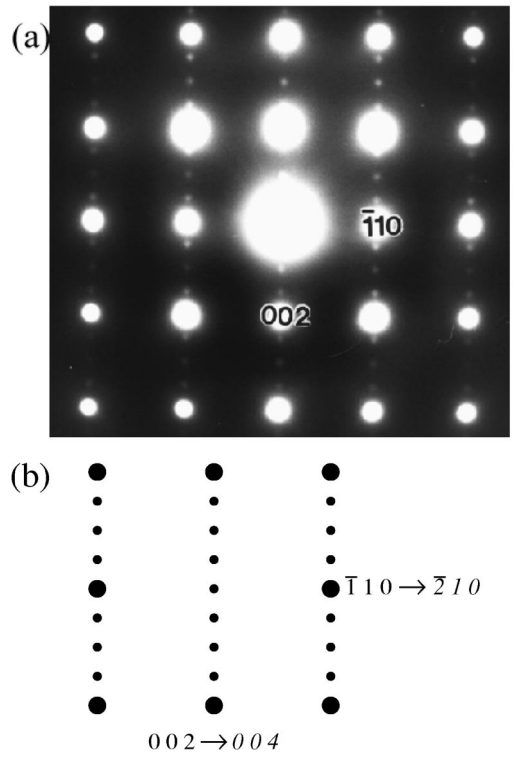

FIG. 2. (a) [110] room temperature ED pattern showing the extra reflections characteristic of the superstructure along c^*. The reflections are indexed in the $I\,bmm$ cell. (b) Indexation of these spots. Italics correspond to indexation in the supercell.

accompanied by a change in the slope of χ^{-1} curves. By fitting Curie laws above and below the transition we have found a change in the effective paramagnetic moment and Curie temperatures from $\mu_{\text{eff}}=4.68(4)\mu_B$/Mn and $\theta_C=+217(5)$ K ($T>610$ K) to $\mu_{\text{eff}}=5.26(2)\mu_B$/Mn and $\theta_C=+104(1)$ K ($T<575$ K).[25] An increment of the effective moment in the low-temperature phase is a characteristic feature of half doped manganites exhibiting CO, and a proper interpretation was given in the framework of the ZPO model.[14] Qualitatively similar changes in the effective magnetic moment have also been reported in $Bi_{0.5}(Ca_{1-y}Sr_y)_{0.5}MnO_3$ for $y=0,0.33,0.67$ and 1.[20] The calorimetry results are displayed in Fig. 1(b), which shows the heat flow obtained when cooling and heating the sample through the transition found by susceptibility data. A moderate hysteresis of about 10 K is visible between the heating and cooling processes. These curves can be adequately integrated thus revealing an entropy change $\Delta s=0.25(1)R$.

A. Electron diffraction

The composition determination was performed by quantitative EDS analysis using a variable spot size and averaging over a large number of crystallites. The cationic analysis evidences a very slight loss of bismuth during the synthesis, but the ratio [(Bi+Sr)/Mn] remains very close to the nominal value. The mean value of the actual cationic composition is $Bi_{0.71\pm0.04}Sr_{0.29\pm0.04}$, calculated for one manganese per unit cell (0.04 refers to the maximum deviation with regard to the average composition). The reciprocal space was reconstructed at RT by tilting around the different equivalent $[100]_P^*$ and $[110]_P^*$ directions of the perovskite sub-cell. This study evidences complex ED patterns, observed for all the crystallites. The system of intense reflections is characteristic of an orthorhombic distorted perovskite sub-cell with $a\approx b\approx\sqrt{2}a_p$ and $c\approx 2a_p$ (a_p is the parameter of the ideal perovskite cell); the conditions of reflection found are hkl: $h+k+l=2n$; $0kl$: $k,l=2n$; $h0l$: $h+l=2n$; $h00$: $h=2n$; $0k0$: $k=2n$; $00l$: $l=2n$. These are consistent with $I\,bmm$ (n. 74) and $I\,bm2$ (n. 46) space groups (SG). Lattice parameters are similar to those reported for $La_{0.5}Ca_{0.5}MnO_3$,[5] and also to those previously reported for the subcell of $Bi_{0.5}Sr_{0.5}MnO_3$, which exhibits at room temperature a supercell related to CO/ZPO.[20,21] Besides the main spots, attributable to the *I*-centered orthorhombic structure, a second set of weaker extra reflections is observed in the ED patterns collected at RT. In order to index them, a doubling of both the *a* and *c* parameters is necessary, i.e., the parameters of the supercell are $a\approx 2\sqrt{2}a_p$, $b\approx\sqrt{2}a_p$, and $c\approx 4a_p$. The observed reflections also imply that there is no condition limiting the reflections. The occurrence of this supercell is illustrated in Fig. 2(a), showing the [110] pattern, and in Fig. 3(a), showing the [001] pattern. Both patterns are equivalent to $\{001\}_P^*$ of the perovskite unit cell and are indexed in the $I\,bmm$ (sub)cell. Schematic drawings of the patterns are given in Figs. 2(b) and 3(b). The indexation of

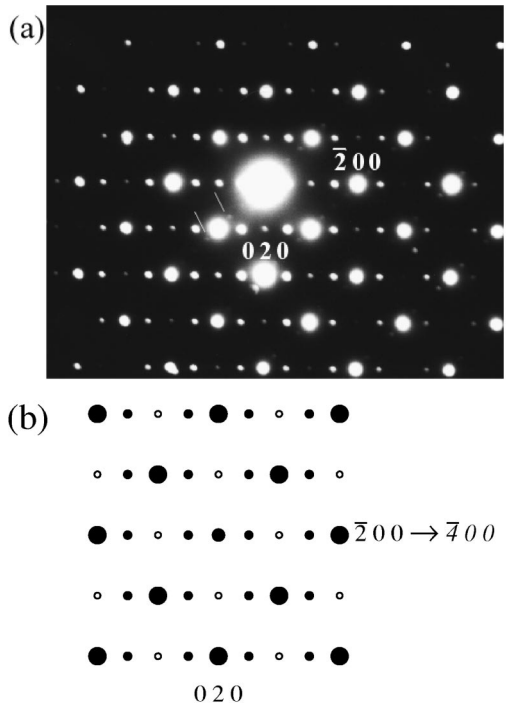

FIG. 3. (a) [001] room temperature ED pattern showing the extra reflections characteristic of the superstructure along a^*. The reflections are indexed in the $Ibmm$ cell. The two small lines point to weak reflections coming from a twinning [110] oriented domain. (b) Indexation of these spots. Italics corresponds to indexation in the supercell.

the reflections in the supercell are indicated in italics. This supercell is similar to that reported for $Bi_{2/3}Sr_{1/3}MnO_3$.[26]

Besides the superstructure (SS), the complexity of the ED patterns is reinforced by the existence of multiple small twinning domains, generated by the orthorhombic distortion of the subcell. This is illustrated in Fig. 3(a) where two very weak extra reflections (shown by white lines) are generated by the presence of a tiny [110] oriented area in the [001] matrix.

B. Synchrotron x-ray and neutron powder diffraction

The results shown above are confirmed by the joint Rietveld analysis of NPD and SXRPD data collected at RT. These data can be jointly refined using $Ibmm$ SG ($R_B = 4.9\%$, $\chi^2 = 2.0$ for SXRPD data and $R_B = 5.1\%$, $\chi^2 = 1.7$ for NPD data), but not using $Ibm2$ SG. The refined patterns are shown in Fig. 4 (the regions of the SXRPD pattern where the diamond peaks are localized have been removed). Together with the (sub)cell reflections a large number of SS reflections can be observed. These have been successfully indexed as satellites of the mean $Ibmm$ structure using propagation vectors $\boldsymbol{k}_1 = (\frac{1}{2}00)$ and $\boldsymbol{k}_2 = (\frac{1}{2}0\frac{1}{2})$ (second line of reflections in Fig. 4). An enlarged view of the SXRPD pattern showing two SS peaks, and their indexes, is plotted in Fig. 5(a). In addition to these peaks, those corresponding to a small impurity of Mn_3O_4 (hausmannite) are also marked in Fig. 4 [the quantitative analysis renders that its fraction is

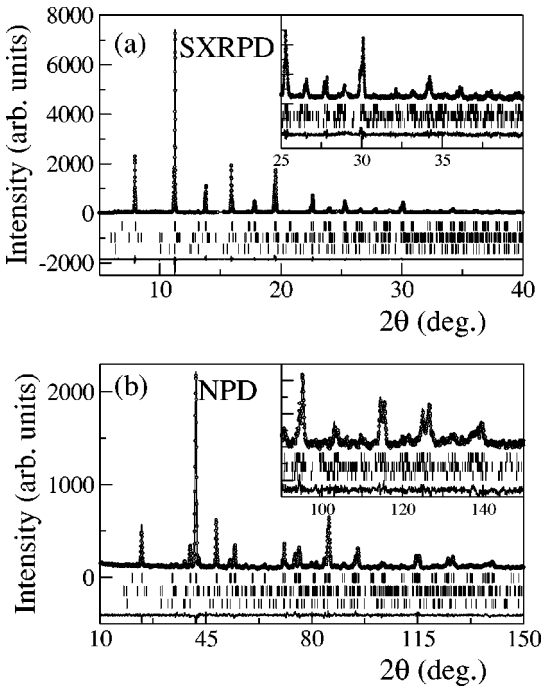

FIG. 4. Joint Rietveld refinement of SXRPD and NPD in the $Ibmm$ SG. The second line of reflections corresponds to SS peaks and the third one to the Mn_3O_4 impurity.

1.5(1)%]. The refinement of the Bi/Sr relation also evidences a small lose of Bi. The composition obtained by the joint Rietveld refinement of NPD and SXRPD data is $Bi_{0.70\pm0.03}Sr_{0.30\pm0.03}MnO_3$, in agreement with EDS analysis. It is worth mentioning that SS spots in Fig. 2 are indexed

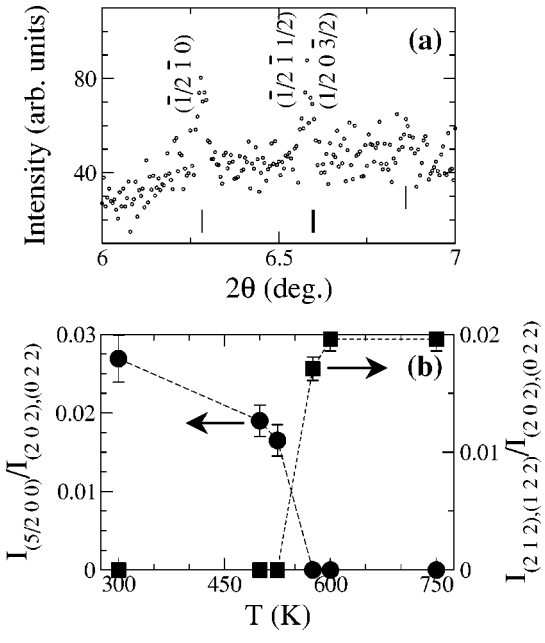

FIG. 5. (a) Small portion of the SXRPD pattern at RT. The two small SS peaks shown are indexed using the two propagation vectors used. (b) Thermal evolution of the integrated intensity of NPD $(\frac{5}{2}00)$ SS peak (left axis) and of the (212)-(122) doublet (violating the I centering), normalized to that of the most intense peak.

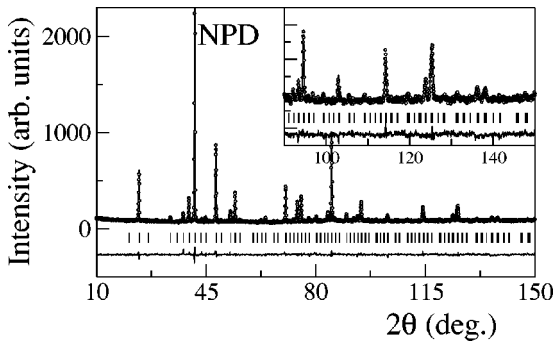

FIG. 6. Rietveld refinement of NPD data at $T=750$ K. The inset shows the high angle region in detail. Data have been refined using *P bnm* SG.

properly with the propagation vector $(0\ 0\ \frac{1}{2})$. We have not detected in the powder-diffraction patterns superstructure peaks with this propagation vector. This is consistent with the weak intensity of SS peaks in Fig. 2 when compared with those in Fig. 3.

Above the transition evidenced by magnetic and calorimetry measurements, the situation is quite different. The NPD diffraction pattern at 750 K can be satisfactorily indexed with a tetragonal [$a=5.53631(5)$ Å and $c=7.8118(1)$ Å] primitive lattice, and no superlattice reflections are found. These reflections disappear (on heating) at about 575 K as is shown in Fig. 5(b). However, the refinement using tetragonal SG's were not satisfactory. The metric of the sample is pseudotetragonal but the symmetry is clearly orthorhombic. The data at $T=750$ K can be very well refined using orthorhombic *P bnm* SG [with $a=5.5386(2)$ Å, $b=5.5310(2)$ Å, and $c=7.8183(3)$ Å, which renders $R_B=6.4\%$ and $\chi^2=1.8$], as shown in Fig. 6. It is worth mentioning that although at low temperature the (sub)cell is *I* centered, several peaks violating the $h+k+l=2n$ reflection condition are found at high temperature. These peaks disappear below 575 K as shown for (2 1 2)-(1 2 2) doublet in Fig. 5(b). The structural details obtained by the Rietveld refinement of NPD data at different temperatures are reported in Tables I and II. Figure 7(a) shows the temperature evolution of the lattice parameters. When entering the low-temperature phase, *a* increases considerably while *b* and *c* slightly decrease. The anisotropic evolution displayed is very different from that found in half doped manganites (typically that of $La_{0.5}Ca_{0.5}MnO_3$) (Ref. 5) where *c* strongly decreases and *a* and *b* slightly increase (in the *P bnm* setting); and also different from that reported in underdoped manganites (for instance $Pr_{0.7}Ca_{0.3}MnO_3$).[9] In contrast, the evolution is very similar to that reported for $LaMnO_3$ when going through the OO transition.[27]

From Table II no significant differences are found between $d_{\text{Mn-O1}}$ and $\langle d_{\text{Mn-O2}}\rangle$ in the studied temperature range. This contrasts with the highly anisotropic evolution (strong apical compression) of Mn-O bond distances in half doped manganites.[5] In the present case, such an anisotropic evolution could be hindered in the average structure, and would only become visible by solving the superstructure. The thermal evolution of $\langle d_{\text{Mn-O}}\rangle$ bond length, Mn-O1-Mn, and Mn-O2-Mn bond angles are shown in Fig. 7(b). It evidences that when entering the low-temperature phase, the MnO_6 octahedron shrinks and that the Mn-O1-Mn bond angle becomes more bent while Mn-O2-Mn is straightened. In contrast with the usual situation in rare-earth manganites, the mobility of e_g electrons is not directly governed by the Mn-O-Mn angle (although $\langle \theta_{\text{Mn-O-Mn}}\rangle$ is near 167° in $Bi_{0.5}Sr_{0.5}MnO_3$ at RT, this compound is insulating).[20]

IV. DISCUSSION

The whole set of results presented indicates that there is a localization of e_g electrons below about 600 K to give an

TABLE I. Structural details obtained by Rietveld refinement of NPD and SXRPD data at RT and from NPD data at $T=500$,525,575,600, and 750 K (average structure). For *I bmm* SG, Mn is on a $4b$ $(\frac{1}{2}\ 0\ 0)$ position, Bi/Sr and O1 are on $4e$ $(x\ 0\ \frac{1}{4})$ position, and O2 on a $8g$ $(\frac{1}{4}\ \frac{1}{4}\ z)$ position. For *P bnm* SG, Mn is placed on $4b$ $(\frac{1}{2}\ 0\ 0)$ position, Bi/Sr and O1 on $4c$ $(x\ y\ \frac{1}{4})$ positions, and O2 on a general $8d$ position.

Temperature		RT	500 K	525 K	570 K	600 K	750 K
SG		*I bmm*	*I bmm*	*I bmm*	*P bnm*	*P bnm*	*P bnm*
a (Å)		5.54244(6)	5.54551(8)	5.54697(7)	5.5274(2)	5.5254(2)	5.5386(2)
b (Å)		5.49907(5)	5.50955(8)	5.51121(7)	5.5165(1)	5.5176(1)	5.5310(2)
c (Å)		7.77022(10)	7.7817(1)	7.7832(1)	7.8010(2)	7.8043(2)	7.8183(3)
V (Å^3)		236.823(2)	237.756(7)	237.937(6)	237.86(1)	237.93(1)	239.50(1)
Bi/Sr	*x*	0.0065(3)	0.0039(6)	0.0042(6)	0.002(1)	0.004(2)	0.000(1)
	y	0	0	0	−0.0075(8)	−0.0091(8)	−0.0081(8)
O1	*x*	0.558(1)	0.5608(8)	0.5596(8)	0.549(1)	0.553(2)	0.550(1)
	y	0	0	0	0.019(1)	0.019(1)	0.019(1)
O2	*x*	$\frac{1}{4}$	$\frac{1}{4}$	$\frac{1}{4}$	0.270(1)	0.273(1)	0.2712(9)
	y	$\frac{1}{4}$	$\frac{1}{4}$	$\frac{1}{4}$	0.2758(7)	0.2740(8)	0.2755(8)
	z	0.0346(5)	0.0331(4)	0.0325(4)	0.0327(6)	0.0317(6)	0.0279(7)
R_B	(NPD)	4.93	6.04	6.10	6.69	7.28	6.37
χ^2	(NPD)	1.74	2.08	1.84	1.85	1.98	1.75

TABLE II. Interatomic bond distances and angles found by Rietveld refinement of diffraction data at different temperatures.

Temperature	RT	500 K	525 K	575 K	600 K	750 K
SG	*I bmm*	*I bmm*	*I bmm*	*P bnm*	*P bnm*	*P bnm*
$d_{\text{Mn-O1}}$ (Å)	1.9690(9)	1.9744(8)	1.9737(7)	1.972(1)	1.975(1)	1.977(1)
$\langle d_{\text{Mn-O2}}\rangle$ (Å)	1.9704(6)	1.9712(4)	1.9711(4)	1.977(4)	1.976(4)	1.977(4)
$\langle d_{\text{Mn-O}}\rangle$ (Å)	1.9699(7)	1.9723(5)	1.9720(5)	1.975(3)	1.976(3)	1.977(3)
$\langle d_{\text{Bi/Sr-O}}\rangle^{IX}$(Å)	2.686(3)	2.690(3)	2.692(3)	2.677(8)	2.677(8)	2.687(7)
$\theta_{\text{Mn-O1-Mn}}$(°)	161.19(4)	160.33(3)	160.73(3)	162.05(4)	161.95(5)	162.65(4)
$\theta_{\text{Mn-O2-Mn}}$(°)(×2)	164.29(2)	164.98(2)	165.27(2)	162.4(2)	162.2(1)	163.4(2)
$\langle\theta_{\text{Mn-O-Mn}}\rangle$(°)	163.26(3)	163.43(2)	163.75(2)	162.3(2)	162.1(2)	163.2(1)

ordered pattern. The first main observation from this study relies on susceptibility data. We have measured an enhancement of μ_{eff} at the transition as predicted by the formation of localized ZP in the low temperature phase.[14] Qualitatively the value of μ_{eff} found above the transition is consistent with a mixture of Mn^{3+} and Mn^{4+} [in a ratio 0.71(4):0.29(4)] $\mu_{\text{eff}}^{\text{theor}}=4.62(4)\mu_B/\text{Mn}$ [$\mu_{\text{eff}}^{\text{exp}}=4.68(4)\mu_B/\text{Mn}$]; and the value found below the transition matches the value that one can expect for the coexistence of ZP and Mn^{3+} ions proposed in Ref. 17. To assess this, let us assume that a fraction α of the manganese ions are in the $3+$ valence state (with $S=2$) and the rest [a fraction $(1-\alpha)$] form ZP (with $S=7/2$). So, for each α Mn^{3+} there will be $(1-\alpha)/2$ ZPs. To find α it is enough to consider the mean valence of Mn ions, which will be $3\times\alpha+3.5\times(1-\alpha)$. So, in the present case [average valence 3.29(4)] it must be $\alpha=0.42(8)$ and then $\mu_{\text{eff}}=\sqrt{\alpha(\mu_{\text{eff}}^{Mn^{3+}})^2+[1-\alpha/2](\mu_{\text{eff}}^{\text{ZP}})^2}=5.32(6)\mu_B/\text{Mn}$ which matches very well with the value found: $\mu_{\text{eff}}^{\text{exp}}=5.26(2)\mu_B/\text{Mn}$. From an ionic CO picture one would expect $\mu_{\text{eff}}^{\text{theor}}=4.62(4)\mu_B/\text{Mn}$. These data indicate that below 600 K many paramagnetic units are not single Mn ions. The fact that there are (almost) no deviations of χ^{-1} curve from the Curie law evidences that these units do not change significantly between 300 and 600 K. The CO/OO picture predicts strong FM coupling inside the FM zig-zag chains of the CE magnetic structure above T_N. This could drive to an apparent μ_{eff} larger than the mentioned value $4.62\mu_B/\text{Mn}$, but the value would display a clear temperature dependence. It must be mentioned that a ''double-rows-type'' contrast was reported in Ref. 26 (for $Bi_{2/3}Sr_{1/3}MnO_3$) and interpreted as an alternating arrangement of Mn^{3+} and polarons in the *a*-*b* plane.

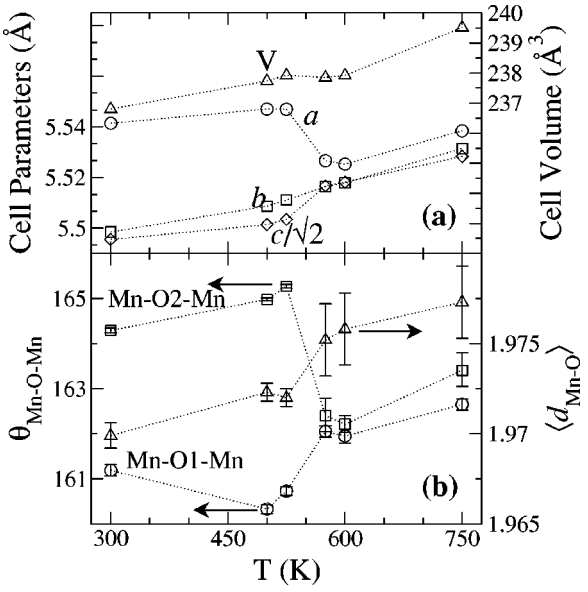

FIG. 7. (a) Anisotropic temperature dependence of the (sub)cell lattice parameters (left axis) and evolution of the unit-cell volume (right axis) through the transition. On cooling, the great expansion of *a* contrasts with the small shrink of *b* and *c*. (b) Temperature evolution of Mn-O-Mn bond angle and Mn-O bond distances from Table II.

From high-resolution NPD and ultra-high-resolution SXRPD data, our $Bi_{3/4}Sr_{1/4}MnO_3$ sample corresponds to a single, well crystallized phase even below the ordering temperature, where we have observed no evidence of phase separation or segregation. To be emphasized is the fact that coexistence of two phases (at RT) has been always found when studying other compositions of the $Bi_{1-x}Sr_xMnO_3$ series such as $x=1/2$ or $x=2/3$.[20,28] This is an indication that the present composition is particularly stable and far from the next most stable composition giving a homogeneous long-range-ordered phase. The well defined structural transition gives rise to a modulated structure (as observed by ED, SXRPD, and NPD at RT) that, in the light of the magnetization data, appears to be more consistent with an ordered pattern of Zener polarons and the remaining ($\approx$40%) manganese atoms in the Mn^{3+} state than with a pure coexistence of Mn^{3+} and Mn^{4+} ions (CO model). The ordered structure doubles *a* and *c* lattice parameters of the (sub)cell. Concomitant with the ordering there is a completely unexpected anisotropic evolution of cell parameters, characterized by a marked expansion (on cooling) of *a*, and a small compression of *b* and *c*. We recall that a similar evolution of the lattice parameters has been recently reported to occur in $Bi_{2/3}Sr_{1/3}MnO_3$, which shows a doubling of *b* and *c* lattice parameters (in the *I bmm* setting).[26] These similarities and the proximity of both concentrations (0.29 and 0.33) indicate that probably both compounds present the same type of ordering. This drives us to the question of which is the ideal doping for the present ground state. It must be mentioned

that the structural changes are more pronounced in the present case and that the structural modulation persists up to higher temperature (it disappears at 500 K for $Bi_{2/3}Sr_{1/3}MnO_3$).[26] In addition to this, DSC measurements on $Bi_{2/3}Sr_{1/3}MnO_3$ render an entropy change $\Delta s = 0.20(1)R$ smaller than the value found in the present case [$\Delta s = 0.25(1)\,R$]. So, we are led to conclude that the degree of order is stronger in $Bi_{0.71(4)}Sr_{0.29(4)}MnO_3$ than in $Bi_{2/3}Sr_{1/3}MnO_3$. Namely, the imperfections, attributable to the nonideal stoichiometry, are smaller in the former than in the latter. Consequently, the ideal composition for this new order or electronic configuration is closer to $x = 0.29$ than to $x = 0.33$.

Now we concentrate on key aspects of the structural changes. ED, SXRPD, and NPD data show that the SG describing the average structure changes from $Pbnm$, characteristic of an $a^+b^-b^-$ rotation of MnO_6 octahedra (in Glazer's notation), to $Ibmm$ resulting in $a^0b^-b^-$ rotation of octahedra,[29] on cooling. The whole set of structural modifications accompanying the transition to the new electronic phase is completely different to that reported for $Bi_{1/2}Sr_{1/2}MnO_3$ and to that usually found in manganites. First, there is a contraction of MnO_6 octahedra [Fig. 7(a)] when entering the CO phase on cooling. This evolution contrasts with the characteristic expansion of Mn-O mean distance during electronic localization in manganites and other transition-metal oxides. However such a contraction has been found in other bismuth containing manganites.[30] In contrast with the $x = 1/2$ case, the electronic reorganization taking place when e_g electrons localize in a single Mn ion or form polarons is not reflected in the Mn-O distances found by fitting the average structure. In the $x = 1/2$ case the basal $\langle d_{\text{Mn-O2}} \rangle$ bond length is significantly larger than the apical $d_{\text{Mn-O1}}$ bond length.[5,31] In the present case there are no differences between these lengths. This dissimilarity can be explained by either the formation of ZP_c (along c axis) or, in the ionic picture, the stabilization of d_{z^2} orbitals (along c axis). In both cases one must expect an apical $d_{\text{Mn-O1}}$ bond distance larger than in the $x = 1/2$ case. It is of interest to underline that, in the present case, *the structural transition does not consist in a slight modulation of the orthorhombic $Pbnm$ high-temperature phase (as commonly found in CO manganites) but in a more pronounced structural transformation that involves a marked symmetry change of the average cell*. Corroborating this fact, the number of observed superstructure peaks is larger (and their intensities higher) than in most common CO Mn perovskites. Unfortunately the description available below the ordering temperature corresponds to the average structure but not to the true (super-)structure, and a definitive picture of the electronic redistribution cannot be drawn precisely.

This new type of ordered structure is more stable (its onset temperature is 600 K) than that of $Bi_{0.5}Sr_{0.5}MnO_3$ (with onset temperature 525 K). It must be noted that this new type of ordered structure has not been reported in rare-earth based manganites, which, in general, are ferromagnetic and metallic or present phase separation, in this compositional range. Thus, it is the fact that bismuth strongly favors the localization of e_g electrons that allows this structure to be formed.

V. CONCLUSIONS

$Bi_{0.71(4)}Sr_{0.29(4)}MnO_3$ displays an ordered localization of e_g electrons at a very high temperature [the onset temperature, from Fig. 1(a), is $T_{ZPO} \simeq 600$ K, the highest ever reported]. The ordering transition is characterized by a change in the SG describing the average structure and by a modulation of the low-temperature phase that doubles a and c lattice parameters of the orthorhombic (sub)cell. This transition is also accompanied by a considerable enlargement of a lattice parameter (while b and c shrinks), by the contraction of the Mn-O bond distance, and by the bending (opening) of Mn-O1-Mn (Mn-O2-Mn) bond angles. It is likely that the same type of order is also present in $Bi_{1-x}Sr_xMnO_3$ with $x = 1/3$,[26] but the present compound is closer to the ideal stoichiometry for this type of order. On the other hand, the structural evolution evidences important differences between the order found and that of half doped $Bi_{0.5}Sr_{0.5}MnO_3$.[20,31] The order found is stronger [$T_{ZPO}(Bi_{0.71}Sr_{0.29}MnO_3) > T_{ZPO}(Bi_{0.5}Sr_{0.5}MnO_3)$] and, in contrast with the $x = 0.5$ and 0.67 cases, the studied sample does not separate into two macroscopic phases at the ordering transition. In order to draw a more detailed picture of the order established at T_{ZPO}, future research, involving the study of the magnetic order at low temperature, is needed. Such description must help us to understand how the polaron ordering takes place in this type of underdoped compounds.

ACKNOWLEDGMENTS

Financial support by the MEC (Grant No. PB97-1175), CICyT (Grant No. MAT99-0984-C03-01), and Generalitat de Catalunya (Grant No. 2001SGR-00334, PICS2001-22) projects is acknowledged. C.F. acknowledges financial support from MCyT (Spain). We thank ILL and ESRF for the provision of neutron and synchrotron x-ray beam times, respectively.

[1] J.B. Goodenough, Phys. Rev. **100**, 564 (1955).
[2] J.W. Verwey, Nature (London) **144**, 327 (1939).
[3] J. Fontcuberta, B. Martínez, A. Seffar, J.L. García-Muñoz, and X. Obradors, Phys. Rev. Lett. **76**, 1122 (1996).
[4] J.L. García-Muñoz, M. Suaaidi, J. Fontcuberta, and J. Rodríguez-Carvajal, Phys. Rev. B **55**, 34 (1997).
[5] P. Radaelli, D. Cox, M. Marezio, and S.-W. Cheong, Phys. Rev. B **55**, 3015 (1997).
[6] P.M. Woodward, D.E. Cox, T. Vogt, C.N.R. Rao, and A.K. Cheetham, Chem. Mater. **11**, 3652 (1999).
[7] J. Blasco, J. García, J.M. de Teresa, M.R. Ibarra, J. Pérez, P.A. Algarabel, C. Marquina, and C. Ritter, J. Phys.: Condens. Matter

9, 10 321 (1997).
[8] O. Richard, W. Schuddinck, G. Van Tendeloo, F. Millange, M. Hervieu, V. Caignaert, and B. Raveau, Acta Crystallogr., Sect. A: Found. Crystallogr. **55**, 704 (1999).
[9] D. Cox, P. Radaelli, M. Marezio, and S.-W. Cheong, Phys. Rev. B **57**, 3305 (1998).
[10] A. Barnabé, M. Hervieu, C. Martin, A. Maignan, and B. Raveau, J. Appl. Phys. **84**, 5506 (1998).
[11] M.T. Fernández-Díaz, J.L. Martínez, J.M. Alonso, and E. Herrero, Phys. Rev. B **59**, 1277 (1999).
[12] P.G. Radaelli, D.E. Cox, L. Capogna, S.W. Cheong, and M. Marezio, Phys. Rev. B **59**, 14 440 (1999).
[13] J. García, M.C. Sánchez, J. Blasco, G. Subías, and M.G. Proietti, J. Phys.: Condens. Matter **13**, 3243 (2001).
[14] A. Daoud-Aladine, J. Rodríguez-Carvajal, L. Pinsard-Gaudart, M. Fernandez-Díaz, and A. Revcolevschi, Phys. Rev. Lett. **89**, 097205 (2002).
[15] J. Rodríguez-Carvajal, A. Daoud-Aladine, L. Pinsard-Gaudart, M.T. Fernández-Díaz, and A. Revcolevschi, Physica B **320**, 1 (2002).
[16] A. Daoud-Aladine, J. Rodríguez-Carvajal, L. Pinsard-Gaudart, M.T. Fernández-Díaz, and A. Revcolevschi, Appl. Phys. A: Mater. Sci. Process. **74**, S1 758 (2002).
[17] A. Daoud-Aladine, Ph.D. thesis, Lab. Léon Brillouin, Saclay, 2001.
[18] C. Frontera, J.L. García-Muñoz, A. Llobet, M. Respaud, J.M. Broto, S. Lord, and A. Planes, Phys. Rev. B **62**, 3381 (2000).
[19] S. Grenier, J.P. Hill, D. Gibbs, K.J. Thomas, M. v Zimmermann, C.S. Nelson, V. Kiryukhin, Y. Tokura, Y. Tomioka, D. Casa, cond-mat/0305216 (unpublished).
[20] J.L. García-Muñoz, C. Frontera, M.A.G. Aranda, A. Llobet, and C. Ritter, Phys. Rev. B **63**, 064415 (2001).
[21] M. Hervieu, A. Maignan, C. Martin, N. Nguyen, and B. Raveau, Chem. Mater. **13**, 1356 (2001).
[22] P. Beran, S. Malo, C. Martin, A. Maignan, M. Nevřiva, M. Hervieu, and B. Raveau, Solid State Sci. **4**, 917 (2002).
[23] N.A. Hill and K.M. Rabe, Phys. Rev. B **59**, 8759 (1999).
[24] A. Calleja, X. Casas, I. Serradilla, M. Segarra, A. Sin, P. Odier, and F. Espiell, Physica C **372**, 1115 (2002).
[25] C. Frontera, J. L. García-Muñoz, C. Ritter, L. Mañosa, X. Capdevila, and A. Calleja, Solid State Commun. **125**, 277 (2003).
[26] M. Hervieu, S. Malo, O. Perez, P. Beran, C. Martin, and B. Raveau, Chem. Mater. **15**, 523 (2003).
[27] J. Rodríguez-Carvajal, M. Hennion, F. Moussa, A.H. Moudden, L. Pinsard, and A. Revcolevschi, Phys. Rev. B **57**, R3189 (1998).
[28] C. Frontera, A. Llobet, M.A.G. Aranda, C. Ritter, and J.L. García-Muñoz, Physica B **276-278**, 793 (2000).
[29] P.M. Woodward, Acta Crystallogr., Sect. B: Struct. Sci. **53**, 32 (1997).
[30] A. Llobet, C. Frontera, C. Ritter, M. Respaud, J. Broto, M. Martínez-Lope, M. Aranda, and J. García-Muñoz, Appl. Phys. A **74**, S1761 (2002).
[31] C. Frontera, J.L. García-Muñoz, M.A.G. Aranda, C. Ritter, A. Llobet, M. Respaud, and J. Vanacken, Phys. Rev. B **64**, 054401 (2001).